Clouds and Shortwave Fluxes at Nauru. Part II: Shortwave Flux Closure

SALLY A. MCFARLANE

Pacific Northwest National Laboratory, Richland, Washington

K. FRANKLIN EVANS

Program in Atmospheric and Oceanic Sciences, University of Colorado, Boulder, Colorado

(Manuscript received 17 November 2003, in final form 24 May 2004)

ABSTRACT

The datasets currently being collected by the Atmospheric Radiation Measurement (ARM) program on the islands of Nauru and Manus represent the longest time series of ground-based cloud measurements in the tropical western Pacific region. In this series of papers, a shortwave flux closure study is presented using observations collected at the Nauru site between June 1999 and May 2000. The first paper presented frequency of occurrence of nonprecipitating clouds detected by the millimeter-wavelength cloud radar (MMCR) at Nauru and statistics of their retrieved microphysical properties. This paper presents estimates of the cloud radiative effect over the study period and results from a closure study in which retrieved cloud properties are input to a radiative transfer model and the modeled surface fluxes are compared to observations.

The average surface shortwave cloud radiative forcing is 48.2 W m^{-2}, which is significantly smaller than the cloud radiative forcing estimates found during the Tropical Ocean Global Atmosphere Coupled Ocean–Atmosphere Response Experiment (TOGA COARE) field project. The difference in the estimates during the two periods is due to the variability in cloud amount over Nauru during different phases of the El Niño–Southern Oscillation (ENSO). In the closure study, modeled and observed surface fluxes show large differences at short time scales, due to the temporal and spatial variability of the clouds observed at Nauru. Averaging over 60 min reduces the average root-mean-square difference in total flux to 10% of the observed flux. Modeled total downwelling fluxes are unbiased with respect to the observed fluxes while direct fluxes are underestimated and diffuse fluxes are overestimated. Examination of the differences indicates that cloud amount derived from the ground-based measurements is an overestimate of the radiatively important cloud amount due to the anisotropy of the cloud field at Nauru, interpolation of the radar data, uncertainty in the microwave brightness temperature measurements for thin clouds, and the uncertainty in relating the sixth moment of the droplet size distribution observed by the radar to the more radiatively important moments.

1. Introduction

In recent years, due primarily to the development of highly sensitive cloud radar systems (Moran et al. 1998; Clothiaux et al. 1999), a large number of liquid cloud optical property retrieval algorithms based on ground-based remote sensing have been developed (Frisch et al. 1995; Dong et al. 1997; Mace and Sassen 2000; McFarlane et al. 2002). Currently, such retrievals are used to develop parameterizations for climate models, to obtain statistics for comparison to cloud and climate model results, to evaluate satellite retrieval algorithms, and to study the microphysical processes such as the aerosol indirect effect (Pincus and Klein 2000; Dong et al. 2002; Feingold et al. 2003).

Algorithms developed to retrieve cloud properties from remote sensing instruments are usually validated by comparing their results against in situ aircraft measurements. However, determining whether these retrievals are realistic in terms of being able to reproduce the radiation budget is also important as that is one of the primary quantities of interest in general circulation models (GCMs). Today most GCMs are tuned to produce correct top of atmosphere albedos [in comparison to the measurements from the Earth Radiation Budget Experiment (ERBE)] by adjusting parameters, such as the effective radius used in optical depth calculations or the threshold value at which autoconversion begins, which may adversely affect the treatment of the hydrological cycle and cloud–radiation feedbacks (Pincus and Klein 2000). Comparing cloud statistics predicted by GCMs to statistics of cloud properties from retrievals, which are shown to reproduce the surface radiation budget, can help assess whether these tunings need to be re-evaluated.

In a companion paper (McFarlane and Evans 2004,

Corresponding author address: Dr. Sally A. McFarlane, Pacific Northwest National Laboratory, P.O. Box 999/MS K9-24, Richland, WA 99352.
E-mail: Sally.McFarlane@pnl.gov

hereafter Part I), we presented retrieved cloud properties from measurements made at the Atmospheric Radiation Measurement (ARM) site on the island republic of Nauru in the tropical western Pacific (TWP). In this paper, we examine whether the retrieved cloud properties are radiatively consistent by performing studies of flux closure at the site. The basic concept of flux closure is that retrieved cloud properties and atmospheric state information are input to a radiative transfer model and then the predicted fluxes from the model are compared to observations.

A few closure studies have considered cloudy sky conditions, although they have been limited to overcast stratus cases only. Zender et al. (1997) compared observed and modeled shortwave surface fluxes for 3 days at the Southern Great Plains (SGP) site during the ARM Enhanced Shortwave Experiment (ARESE). They found good agreement between the model and measurements for 2 clear-sky days (model overestimating surface fluxes by approximately 11 and 17 W m^{-2}), but a much larger offset (model overestimating surface flux by 62 W m^{-2}) for a cloudy case. The clear-sky day with flux difference of 11 W m^{-2} was much less turbid with average aerosol optical depth of 0.004, compared to 0.12 for the other clear-sky day. The large differences for the cloudy day could be due in part to the lack of information about the aerosol properties. Additionally, the Malkmus band model used in the absorption calculations has been shown to underestimate gaseous absorption in inhomogeneous atmospheres (Warner and Ellingson 2000) and questions have been raised about the accuracy of some of the radiometers during the experiment (Li et al. 1999). Results from the ARESE II experiment, conducted at the SGP site during March 2000 found agreement in measured and calculated absorption to within 10% for 2 clear-sky days and two single-layer stratus cases, and agreement within 8%–14% (depending on surface albedo) for a third stratus case (Ackerman et al. 2003). In these calculations, state-of-the-art radiative transfer models that used the *k*-distribution or exponential sum methods to calculate gaseous absorption were used. The primary uncertainties in the modeled fluxes were surface albedo and aerosol optical thickness.

In the few cloudy sky closure experiments that have been performed, the emphasis has been on a case study approach in which modeled and measured fluxes are compared for specific, limited time periods, in which only overcast stratus clouds are present. This paper presents a shortwave flux closure study with a different focus. Instead of concentrating on a few case study periods, we perform flux closure in a more statistical sense by comparing the statistics of modeled and measured fluxes over long time periods. The primary objective of the study is to examine whether cloud optical properties retrieved from narrow field of view (FOV), vertically pointing remote sensors are consistent with the measured surface radiation budget in a statistical sense.

In section 2 we discuss the observations and retrieved cloud properties while section 3 describes the radiative transfer model and details of the flux calculations. In section 4 we present the clear-sky modeling results and estimates of the shortwave cloud radiative effect at the surface. In section 5 we present results and discussion from the flux closure experiment, and in section 6 we examine reasons the radar cloud amount might be larger than the radiative cloud amount. Finally, section 7 summarizes the study.

2. Observations and retrieved cloud properties

a. Shortwave radiation measurements

The Atmospheric Radiation and Cloud Station (ARCS) on Nauru (Mather et al. 1998) includes three upward-looking shortwave radiometers: an unshaded Eppley Precision Spectral Pyranometer (PSP), which measures total hemispheric downwelling irradiance; a shaded Eppley PSP, which measures diffuse downwelling irradiance; and an Eppley normal incidence pyrheliometer (NIP), which measures the direct component of the solar flux at normal incidence in a 5.7° FOV. All three instruments are located on the same stand, 1.5 m above ground level, with the same solar tracker used for the NIP and the shaded PSP. All of the shortwave radiation measurements at the ARCS are reported as 1-min averages of samples taken each second.

Michalsky et al. (1999) examined surface shortwave irradiance measurements with commercial instrumentation and found that measurement accuracy was improved to 1%–2% of total downwelling solar irradiance if the ''component sum'' method was used instead of single unshaded pyranometers. The component sum method consists of summing the diffuse irradiance from a shaded pyranometer and the direct normal irradiance from a pyrheliometer multiplied by the cosine of the solar zenith angle. This method reduces the effect of the cosine response of the unshaded pyranometer. Following Michalsky et al. (1999) all total observed fluxes discussed in this paper are calculated via the component sum method. Long and Ackerman (2000) estimate uncertainties in total and diffuse downwelling clear-sky shortwave pyranometer measurements for long-term operational measurements to be no better than the greater of 15 W m^{-2} or 3% of the flux. The stated uncertainty on the direct flux measured by the NIP is 4 W m^{-2} or 3% of the downwelling flux.

The Eppley pyranometers exhibit a dome thermal offset in which infrared heating exchanges within the instrument can cause a spurious voltage signal. This offset can be directly observed in the measurements at night, and can be estimated for daytime based on monitoring the temperature of the case and dome of the pyranometer or using measurements from an adjacent pyrgeometer (Haeffelin et al. 2001). Based on the magnitude of nighttime offsets at Nauru (generally less than 1.5 W m^{-2}),

the maximum daytime offset is expected to be no more than 5 W m^{-2} (C. N. Long 2002, personal communication). Due to the small offsets expected at Nauru, we perform no thermal offset corrections on the PSP data.

b. Aerosol measurements

Aerosol measurements are taken by the Cimel sun photometer on Nauru, which is part of the the Aerosol Robotic Network (AERONET) archive (http://aeronet.gsfc.nasa.gov.). The archive contains data for Nauru from 15 June 1999 through 11 April 2000. Retrievals of aerosol optical thickness are performed in seven spectral bands between 340 and 1020 nm. The aerosol optical thickness (AOT) at Nauru is typically low, with values at 550 nm generally less than 0.15, and an average and standard deviation of 0.071 and 0.030, respectively, during this period. To estimate AOT for each band in the radiative transfer calculations, we perform a multiple linear regression on the AOT in the channels from 440 to 870 nm to calculate the Ångstrom parameter for each measurement (Smirnov et al. 2002). Then we calculate the AOT at the solar-weighted center wavelength of each model band using the derived Ångstrom parameter and interpolate the AOT to a 30-min time grid.

We characterize the aerosol size distribution by the average bimodal lognormal distribution as retrieved by Smirnov et al. (2002) from Cimel diffuse sky measurements at Nauru between 15 June 1999 and 9 September 2000. Most of the aerosol volume is found to be in the coarse mode, which is defined to be particles with radii between 0.6 and 16 μm. Values of the single scattering albedo and refractive index are taken from d'Almeida et al. (1991) assuming the ''oceanic'' aerosol model, which is a mixture of sea salt and organic sulfate. In comparison with four other marine locations studied by Smirnov et al. (2002), Nauru had the smallest volume concentration of particles in the fine mode, supporting the assumption that aerosols at Nauru are primarily oceanic and not industrial.

Although stratospheric aerosol amounts are fairly small due to the lack of recent volcanic eruptions, we include stratospheric aerosol in the model. Total stratospheric AOT is determined from Stratospheric Aerosol and Gas Experiment (SAGE) II data, and is approximately 0.005 at 500 nm. We assume the stratospheric aerosol consists entirely of sulfate and exists in a uniform layer between 17 and 40.5 km. Optical properties of sulfate aerosol are taken from d'Almeida et al. (1991).

c. Retrieved cloud properties

The cloud property retrievals are discussed in detail in Part I. Cloud phase is determined from a simple temperature threshold, clouds having tops at temperatures above -10°C are assumed to be liquid clouds, while all others are assumed to be ice. Times when the optical rain gauge data measurements are greater than 0.05 mm h^{-1} and times when the maximum radar reflectivity in the column is greater than 0 dBZ for liquid clouds are assumed to be periods of precipitation and are not included in the closure experiment. For nonprecipitating liquid clouds, vertical profiles of liquid water content and effective radius are calculated from microwave radiometer (MWR) brightness temperatures and millimeter wave cloud radar (MMCR) reflectivies using the Bayesian retrieval algorithm developed by McFarlane et al. (2002). Unless stated otherwise, the radar reflectivities are from the Active Remote Sensing of Cloud Layers (ARSCL) dataset, described by Clothiaux et al. (2000).

Due to problems with the micropulse lidar (MPL) during the study period, only ice clouds detected by the MMCR are used in the closure studies. Although the radar misses high thin cirrus (see discussion in Part I), these clouds have only a small impact on the surface fluxes (McFarquhar et al. 2000). For ice phase clouds, profiles of ice water content (IWC) and effective diameter are calculated from radar reflectivity using regression equations as a function of temperature, which were derived from the Central Equatorial Pacific Experiment (CEPEX) and which were described in Part I. McFarquhar and Heymsfield (1996) studied three tropical anvils sampled during the CEPEX experiment and found that aggregates were common when IWC was greater than 0.1 g m^{-3} and that plates and columns were noticed for lower IWC. Thus, for layers with IWC $>$ 0.1 g m^{-3}, the particles are assumed to be smooth aggregates, and for layers with lower IWC, the particles are assumed to be plates. The choice of plates instead of columns for the layers with low IWC has only a small impact on the modeled surface fluxes and does not substantially affect any of the results presented.

d. Data quality issues

From 6 August through 14 October 1999, the Nauru solar tracker was not operational. A new tracker was installed on 14 October, and usable data are available again beginning 18 October 1999 (R. Perez 2001, personal communication). The malfunction of the solar tracker affects the data from the NIP and shaded PSP. We do not use any radiation data from this period. The solar tracker began to malfunction again on 23 March 2000. From this time to the end of the study period, the solar tracker did not work correctly around solar noon, and the fluxes measured during this half hour cannot be used, but the rest of the data is reliable. Examining the unshaded PSP measurements, which are not affected by the malfunctioning of the solar tracker, shows that removing the times around noon for this period does not bias the average shortwave cloud effect estimates presented later.

A peak in the MWR brightness temperatures around local solar noon was noticed during the periods 14 Sep-

TABLE 1. Dates and times with missing or unusable data.

Data	Times affected	Instrument
6 Aug 1999–14 Oct 1999	All times	PSP, NIP
14 Sep 1999–6 Oct 1999	2 h around noon	MWR
20 Dec 1999–17 Jan 2000	All times	MMCR
7 Mar 2000–30 Mar 2000	2 h around noon	MWR
23 Mar 2000–End	30 min around noon	PSP, NIP

tember through 6 October 1999 and 7 March through 30 March 2000. This peak in brightness temperatures is due to solar contamination of the MWR signal around the equinox periods, at which times the sun would be directly overhead around solar noon at Nauru. Data from the MWR for the 2 h around noon during these periods are not used. The MMCR had sporadic problems throughout the study period, the longest being a time period between 20 December 1999 and 17 January 2000 in which the radar data were invalid. Table 1 summarizes the dates and times with missing data during the study period. For times when the MWR or MMCR data are missing, cloud properties are not retrieved and closure calculations are not performed; however, these times are included in the estimates of cloud radiative effect. If the NIP or PSP data are missing, the times are not used at all.

3. Details of radiative transfer model and flux calculations

a. Radiative transfer model

Broadband downwelling fluxes at the surface are calculated using the Spherical Harmonics Discrete Ordinates Method (SHDOM) model (Evans 1998) in plane-parallel mode and incorporating the Rapid Radiative Transfer Model (RRTM) correlated-*k* distribution (Mlawer et al. 1997). The extinction, single scattering albedo, and Legendre coefficients of the scattering phase function are specified for each wavelength band at each input grid point. The RRTM correlated-*k* distribution has 13 bands in the shortwave region applied to 0.2–3.84 μm. The absorption coefficients are provided by the line-by-line radiative transfer model (LBLRTM; Clough and Iacono 1995) and based on the 1992 high-resolution transmission (HITRAN) parameter database and the Clough–Kneizys–Davies (CKD) 2.2 water vapor continuum model (Clough et al. 1992). Comparisons of direct-beam surface flux (no Rayleigh extinction) calculations in the shortwave from RRTM and LBLRTM agree to within 1 W m^{-2} for clear sky (Mlawer et al. 1998).

Liquid cloud optical properties are calculated for each band using Mie scattering theory from a vertical profile of liquid water content and effective radius. Optical properties for cirrus clouds are calculated from parameterized scattering properties of individual ice crystals (Yang et al. 2000). Bulk scattering properties are obtained by integrating the single scattering properties of individual crystals over a normalized gamma distribution with a given effective diameter and total ice water content. Only one particle shape per ice layer is allowed.

SHDOM can be run with arbitrary angular and spatial resolution, allowing a trade-off between speed and accuracy. The angular accuracy is controlled by the number of radiation streams chosen, and the spatial resolution by a parameter called the splitting accuracy, which governs when a grid cell is split in half. Due to the large time series of data processed in this study, we use six radiation streams, and a splitting accuracy equal to 0.01% of the incident solar flux in each band. Compared to a reference case in which 32 streams were used, this leads to a total broadband error of less than 2.5 W m^{-2}, or 0.7% of the calculated downwelling flux, for a range of clouds with optical depths between 1 and 50.

The surface albedo of the Nauru site is quite complicated, with the radiometers located on a bright, sandy beach immediately adjacent to the dark ocean. During the Nauru99 experiment, the University of Flinders' Cessna aircraft made several low flights to characterize the albedo of the island. The broadband albedo determined from the ratio of the upwelling and downwelling unshaded PSPs on board the Cessna ranged from 0.03 over the ocean to 0.15 over the island interior and 0.3 over the beaches. Based on these values and estimates of distance from maps and photographs of the island, a simple schematic of albedo variability over the island was developed. Two-dimensional (2D) flux calculations were performed with SHDOM for clear sky and for several low clouds of varying optical depths using this variable albedo surface. Then 1D flux calculations with varying average albedos were performed. An average 1D albedo value of 0.13 was found to best match the 2D flux calculations, and was used as a typical value for the site.

The temperature and humidity profiles for input to the radiative transfer model are determined from the nearest radiosonde, which are typically launched twice per day at Nauru. The temperature in the Tropics is not expected to vary greatly on time scales of several hours. Due to the dry bias in the radiosonde humidity measurements and the infrequency of radiosonde launches, 30-min averages of the Bayesian precipitable water vapor (PWV) retrievals, obtained from the MWR brightness temperatures, are used to scale the radiosonde water vapor profile. The total ozone column amount is estimated from the Total Ozone Mapping Spectrometer (TOMS) instrument on the *Earth Probe* satellite, and the McClatchey et al. (1972) tropical atmosphere profile is used for the ozone vertical distribution profile.

b. Flux calculations

Due to the large dataset being studied, the speed of the radiative transfer (RT) calculations is increased by averaging the retrieved cloud properties to 1-min res-

olution to match the time scale of the reported flux observations. Additionally, calculations of the gaseous absorption with the correlated-*k* distribution method are performed only once every 30 min, using the atmospheric temperature and humidity profile from the closest radiosonde, the ozone profile, and the average retrieved PWV over the interval. These absorption coefficients are then used in the 1-min RT calculations. To account for broken cloudiness within the 1-min interval, one RT calculation is performed on the average cloud properties over the cloudy columns, and one RT calculation is performed on a clear column and a weighted average of the calculated fluxes is taken. If the 1-min period is entirely clear or entirely cloudy only one flux calculation is performed.

If 10% or more of the 1-min periods are invalid (i.e., precipitation is occurring or data are missing or unusable) during the 30-min period, none of the radiative transfer calculations are performed for the 30-min period; if fewer than 10% are invalid, cloud properties are interpolated over any invalid columns. Calculations of the the total, direct, and diffuse downwelling flux are performed each minute of the 30-min period.

c. Direct/diffuse partition of flux

Theoretically, the direct component of the shortwave radiation field is that part which has not been scattered, while the diffuse component consists of light that has been scattered at least once. In the model calculations, the separate contributions of the direct and diffuse components to the total flux can be easily calculated. However, in the observations the determination of the direct and diffuse components is not as straightforward. The NIP has an FOV of 5.7°, and thus actually measures the direct component of the solar radiation plus any of the diffuse component that is scattered into this field of view. In order to compare the ''direct'' component between the model and the observations, the model calculations must be corrected to account for forward scattering into the FOV of the NIP. For clear sky, this correction is rather small, although it does depend on the aerosol loading. Halthore et al. (1997) estimate the correction to be about 0.1% of the measured direct beam for the aerosol conditions they studied. Since forward scattering increases with increasing particle size (relative to wavelength), scattering into the field of view of the NIP is more important under conditions of thin clouds.

Following the study of Shiobara and Asano (1994), we use a Monte Carlo model to examine the amount of scattering into the FOV of the NIP as a function of optical depth, particle size, and particle habit. A maximal cross section forward Monte Carlo code, which includes the shortwave RRTM *k* distribution, is modified to simulate the broadband (i.e., 0.2–3.486 μm) flux measurement of a narrow field-of-view (NFOV) instrument with halfwidth η. Every photon that reaches the surface with an angle within η of the direct beam is assumed to contribute to the flux measured by the instrument. The amount of flux scattered into the FOV of the instrument depends strongly on the cloud optical depth, particle phase, and particle size. In Fig. 1, we compare the modeled NFOV flux transmittance to the calculated direct beam (unscattered) flux transmittance as a function of cloud visible optical depth for several liquid and ice clouds. In these calculations, no Rayleigh scattering or atmospheric absorption were included. Also shown are the transmittance values calculated by Shiobara and Asano (1994) for a sun photometer with a 2.4° field of view using the Takano and Liou (1989) phase function.

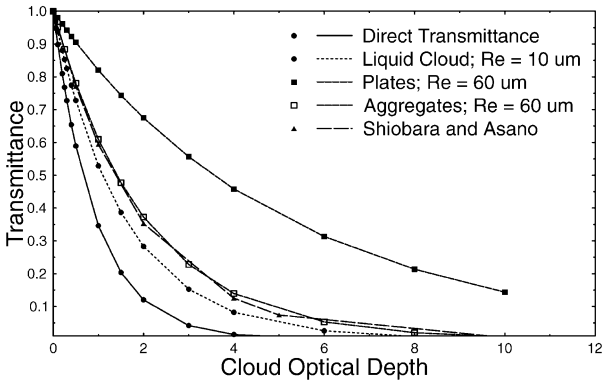

FIG. 1. Direct beam flux transmittance (solid line) and modeled narrow field of view transmittance as a function of optical depth for several model clouds. Also shown is the parameterization of Shiobara and Asano (1994).

To correct the modeled values of direct and diffuse flux in the closure experiment, a lookup table is developed that relates the modeled instrument flux transmittance to the cloud slant path visible optical depth, mass-weighted average effective radius, and column water vapor amount. For each 1-min period, the transmittance into the FOV of the instrument $\mathcal{T}_{\mathrm{FOV}}$ is estimated from the lookup table. The magnitude of the flux correction is given by $\Delta F = F_{\mathrm{TOA}}\mathcal{T}_{\mathrm{FOV}} - F_{\mathrm{DIR}}$, where F_{TOA} is the broadband flux at the top of the model atmosphere and F_{DIR} is the calculated direct flux at the surface. The value of ΔF is subtracted from the modeled diffuse flux and added to the modeled direct flux. The modeled total flux is unchanged. Over the study period, the average amount of the correction over all cloudy columns is 38.4 W m^{-2}. All of the following results and discussion use the corrected model fluxes.

4. Cloud radiative effect estimates

In Part I, statistics of the observed clouds at Nauru were presented. In this section we examine the effect of the clouds on the surface shortwave fluxes at Nauru. The cloud radiative effect at the surface is estimated by comparing the observed shortwave fluxes at the surface to modeled clear-sky fluxes.

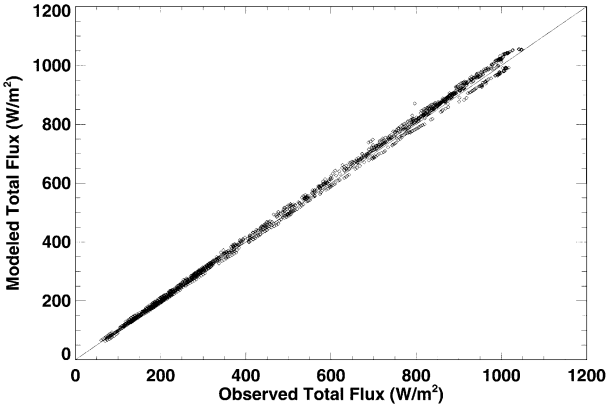

FIG. 2. Comparison of measured and modeled total downwelling flux for times determined to be clear by the analysis method of Long and Ackerman (2000).

a. Clear-sky results

The MMCR and MPL detect clouds, on average, 70% of the time at Nauru. Thus the sky should be clear 30% of the time directly above the remote sensors. However, even when there are no clouds within the narrow fields of view of the radar and lidar, there are likely to be clouds in other parts of the sky, which may affect the measured fluxes. To evaluate the clear-sky modeling, we compare modeled and observed fluxes for times when the shortwave flux analysis method developed by Long and Ackerman (2000) indicates clear skies within a 160° field of view. Over the study period, 1261 measurements over 40 different days fit the criteria for clear-sky identification. Figure 2 shows a scatterplot of the measured and modeled total downwelling fluxes for these times. In these comparisons, the results are presented as modeled minus measured fluxes, so that a negative flux difference is a model underestimate of downwelling flux at the surface. The average total flux difference is 7.2 W m^{-2} (0.6% of observed total flux), with a root-mean-square (rms) difference of 14.4 W m^{-2}. The average direct flux difference is -10.4 W m^{-2} (2.2% of average observed direct flux), and the average diffuse flux difference is 17.2 W m^{-2} (26.3% of observed diffuse flux).

The disagreement in diffuse flux is of the the same sign and order of magnitude found in other clear-sky studies (Halthore et al. 1997; Kato et al. 1997; Mlawer et al. 2000; Halthore and Schwartz 2000). While we had hoped that the remoteness of Nauru would make the aerosol properties simpler, thus simplifying the closure inputs, this appears not to be the case. Clear-sky diffuse fluxes are sensitive to AOT, aerosol properties, and surface albedo, all of which are fairly uncertain. The broadband AOT must be estimated from the narrowband sun photometer measurements. The aerosol optical properties are assumed to be representative of ''clean'' oceanic aerosols, containing only sea salt and sulfate. Measurements of surface aerosol properties during Nauru99 indicated the existence of ammonium, phosphate, and nitrate as well, which are due to the phosphate mining on Nauru and the loading of phosphate onto ships. The surface albedo of the Nauru site is quite complicated, with the radiometers located on a bright, sandy beach immediately adjacent to the dark ocean. While the variability of the surface albedo was taken into account in setting the albedo used in the model, more detailed observations of the 2D variability in albedo would provide more realistic values. Although the difference in diffuse flux is relatively large, given the small values of diffuse flux under clear sky (average observed value 65.2 W m^{-2}), it is less than 4% of the total clear-sky flux.

TABLE 2. Average observed all sky downwelling flux, modeled clear-sky downwelling flux, and estimated shortwave cloud radiative effect at the surface for all data and morning and afternoon periods.

		Total (W m^{-2})	Direct (W m^{-2})	Diffuse (W m^{-2})
All data	Cloud radiative effect	−55.4	−150.4	95.0
	Observed all-sky flux	532.3	361.9	170.4
	Model clear-sky flux	587.7	512.3	75.5
Morning	Cloud radiative effect	−41.9	−132.2	90.3
	Observed all-sky flux	544.7	378.6	166.1
	Model clear-sky flux	586.6	510.8	75.8
Afternoon	Cloud radiative effect	−68.4	−167.9	99.5
	Observed all-sky flux	520.4	345.7	174.6
	Model clear-sky flux	588.8	513.7	75.1

b. Cloud radiative effect estimates

We calculate the clear-sky-modeled fluxes for all times for which we have valid observed fluxes. We define the shortwave cloud radiative effect at the surface as the observed downwelling shortwave flux at the surface minus the modeled clear-sky downwelling shortwave flux at the surface. A negative value indicates that cloud has reduced the downwelling flux at the surface relative to the clear-sky value. Table 2 gives the average observed and modeled clear-sky fluxes and the average shortwave cloud radiative effect at the surface for the entire dataset and separated by morning and afternoon.

Over the entire period, the average radiative effect of clouds on the total downwelling shortwave flux is -55.4 W m^{-2}, which is roughly 10% of the average modeled clear-sky flux. Observations taken during the Nauru99 field experiment showed that the island of Nauru tended to induce cloud formation, in the form of a ''cloud plume'' in which shallow cumulus clouds formed directly over or slightly downwind of the island and then were advected further downwind by the mean winds. Nordeen et al. (2001) examined a year of Geostationary Meteorological Satellite (GMS) hourly visible 1.25-km images over Nauru between 15 June 1999 and 30 June 2000 to study the cloud plumes. They observed unobscured cloud plumes in 53% of days with a complete record of GMS visible images. Cloud plume frequency increases from roughly zero at 0630 local

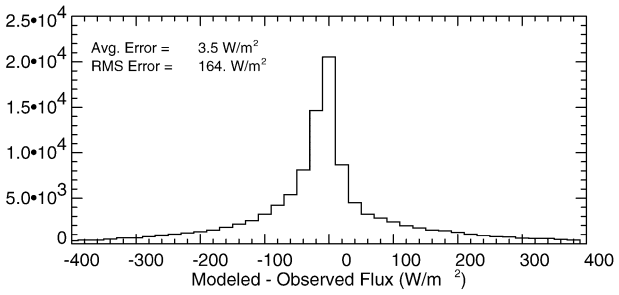

FIG. 3. Histogram of 1-min total downwelling flux differences.

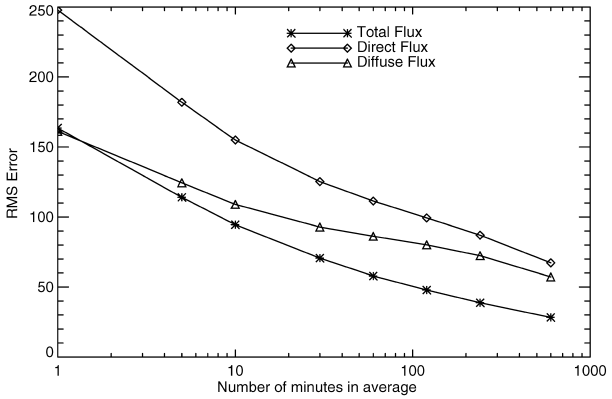

FIG. 4. Root-mean-square differences in modeled and observed flux as a function of averaging time.

standard time (LST) to 63% at 1130 LST, and remains roughly constant until sunset. While the average modeled fluxes for the morning and afternoon periods are roughly equal, the average observed total flux is 24 W m^{-2} lower in the afternoon period. The average radiative effect of clouds on the total downwelling shortwave flux during the morning is -43.3 W m^{-2}, compared to -68.4 W m^{-2} in the afternoon, which may be due in large part to the island-induced clouds seen at Nauru, which are more frequent in the afternoon.

To relate the cloud radiative effect estimates to the estimates of shortwave cloud radiative forcing (CRF) at the surface performed by other groups, we assume that clear-sky and all-sky albedos are equal, and multiply our cloud radiative effect estimates by $(1 - \alpha)$, where $\alpha = 0.13$ is the assumed albedo at Nauru. Thus, our average estimated cloud radiative effect of -55.4 W m^{-2} is roughly equal to a CRF of 48.2 W m^{-2}. This value is smaller than average cloud radiative forcing estimates for the Tropical Ocean Global Atmosphere Coupled Ocean–Atmosphere Response Experiment (TOGA COARE) period. Chou and Zhao (1997) estimate an average shortwave CRF of 112 W m^{-2} at Nauru over the 4 TOGA COARE months, November 1992–February 1993. Their average estimated shortwave CRF over the seven radiation stations (including the two research ships) was 99 W m^{-2}. Long (1996) does not calculate the average CRF at Nauru; however, he estimates an average area-weighted shortwave CRF of 98 W m^{-2} over the five sites in the inner flux array. The differences in estimates of the average shortwave cloud radiative forcing at the surface in these studies compared to our results is most likely due to variability in cloud amount between the TOGA COARE period (which was during the weak phase of El Niño) and the current study period (which was during a weak to moderate La Niña). During El Niño periods, the region of active convection generally shifts to the east, and there was more convective activity over Nauru during the TOGA COARE period than during this study period [based on examination of the average outgoing longwave radiation from the National Centers for Environmental Prediction (NCEP) reanalysis product for these periods].

5. Initial flux closure results

In the previous section we showed that the model does a reasonable job of replicating the clear-sky flux. Now we examine our ability to reproduce the cloudy sky fluxes observed at Nauru. We perform flux closure on the retrieved cloud properties for all nonprecipitating and nondrizzling clouds between 15 June 1999 and 11 April 2000. For this period, we perform radiative transfer calculations on 93 232 min of data, of which 47.7% have no cloud detected by the radar (but may contain thin cirrus detectable by the lidar), 32.2% are liquid clouds, 12.5% are radar-detected ice clouds, and 7.3% contain both liquid and radar-detected cirrus clouds. In the discussion that follows, all flux differences refer to model fluxes minus measured fluxes, so that a negative flux difference is a model underestimate of downwelling flux at the surface.

A histogram of the differences of the 1-min averages of total downwelling flux over the study period is shown in Fig. 3. The average difference in the total flux over the entire study period is only 3.5 W m^{-2}, although the rms error is 164 W m^{-2}. To put the magnitude of these errors in context, the mean observed downwelling flux for this period is 553.3 W m^{-2}. These results indicate that, on average, the model total flux is unbiased, although there is large variability in the results. The spread in the histogram is due to the large temporal variability of the clouds at Nauru. Many of the nonprecipitating clouds observed at Nauru are shallow cumulus which advect fairly quickly over the site, leading to large numbers of broken cloud scenes. Out of 2855 30-min periods, only 31% had radar detected cloud frequencies (fraction of 1-min intervals during which clouds are detected by the MMCR) greater than 90%. By averaging the observed and modeled fluxes over longer time periods, the variability in the flux differences can be reduced. Figure 4 shows the rms differences in total flux as a function of averaging time. After averaging both the modeled and observed fluxes over 30 min, the rms difference has been reduced by half, and over 60 min

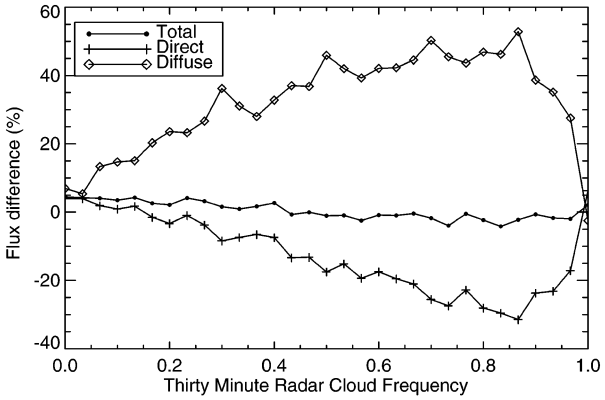

FIG. 5. Relative differences in total, direct, and diffuse flux for 30-min periods as a function of radar-observed cloud frequency.

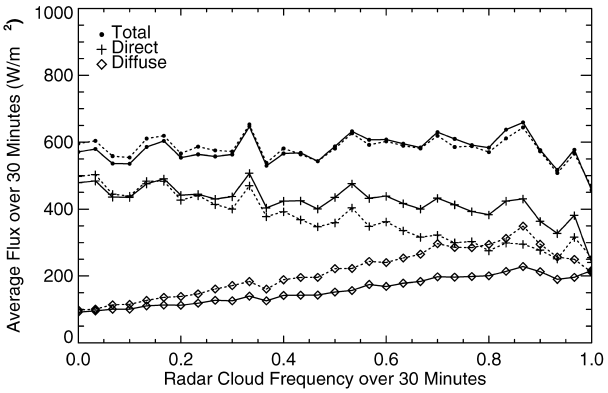

FIG. 6. Average observed and modeled flux over 30-min periods as a function of radar-observed cloud frequency. Solid lines indicate observed values, while dashed lines indicate modeled values.

the rms difference in total flux is 57.9 W m^{-2}, or 10.4% of the observed value.

Also shown in Fig. 4 are the rms differences for the direct and diffuse fluxes. Although they also decrease substantially with averaging time, the rms differences in direct and diffuse flux are significantly larger than those in the total flux. The relatively good agreement in total flux is caused in part by corresponding under- and overestimates of direct and diffuse fluxes, respectively. The model underestimates direct flux by an average of -38.0 W m^{-2} and overestimates diffuse flux by 41.5 W m^{-2}.

The model flux errors depend strongly on the retrieved cloud amount (Fig. 5). We average the observed and modeled fluxes over 30-min periods and use the radar-observed frequency of occurrence of clouds as a determination of cloud amount. In section 4a we found that during periods identified as clear sky by the Long and Ackerman (2000) shortwave flux analysis method, the model underestimated the direct flux by 2.3% and overestimated the diffuse flux by 26%. However, for periods designated as clear sky by the radar, the model overestimates the direct fluxes by ~10% and overestimates the diffuse flux by 5%. This is due to the fact that a 30-min period of clear sky over the radar does not necessarily indicate that the entire sky is clear. Clouds not detected by the radar will decrease the observed direct flux and decrease the observed diffuse flux relative to the model values.

For cloud frequencies greater than 0 and less than 0.9, the magnitude of the direct and diffuse errors both increase with increasing cloud frequency while the errors in total flux stay relatively constant. The abrupt change in the direct and diffuse errors at cloud frequencies greater than 0.9 is due to the fact that high cloud frequencies are most often observed when radar detected ice clouds are present. For periods with cloud frequency between 0.1 and 0.9, the mean frequency of occurrence of radar ice clouds (including liquid clouds with ice clouds above) was 0.06, while for the periods with cloud frequency greater than 0.9, the mean frequency of occurrence of radar ice clouds was 0.56. The model actually tends to overestimate direct flux and underestimate diffuse flux for periods when only ice clouds are present. This is due in part to a small overestimate of the NFOV correction from assuming the cirrus are composed of plates, which have more forward scattering, and thus a larger NFOV correction, than other crystal habits (Fig. 1).

The trend in model errors as a function of cloud frequency at intermediate values is harder to understand. In general, any time there is cloud in the model, the direct flux will be reduced relative to clear sky and the diffuse flux will be enhanced. So, if cloud is detected by the radar, but is not in the field of view of the NIP, the model would overestimate the diffuse flux and underestimate the direct flux, as seen. However, if the cloud field is isotropic, it is equally likely that there would be cloud in the field of view of the NIP that is not detected by the radar.

In Fig. 6, the 30-min average observed and modeled fluxes are plotted as a function of radar-observed cloud frequency. For low cloud frequencies, the observed and modeled direct fluxes agree fairly well but the model slightly overestimates the diffuse flux. As expected, as the radar cloud frequency increases, the average-observed direct fluxes tend to decrease (higher probability of cloud in the direct beam) and the average-observed diffuse fluxes tend to increase (higher cloud fraction enhances the observed diffuse flux). The modeled fluxes show the same trend as the observed fluxes (the cloud frequency does not affect the model results for each individual minute, but as cloud frequency increases the average values change due to the increased number of cloudy sky points in the average). However, the rate of change with cloud fraction is higher for the model results. At a radar cloud frequency of 1.0 the observed and modeled fluxes converge to the same value.

These results indicate that the retrieved cloud frequency and the radiative effective cloud fraction do not agree for conditions of less than full cloud cover. The

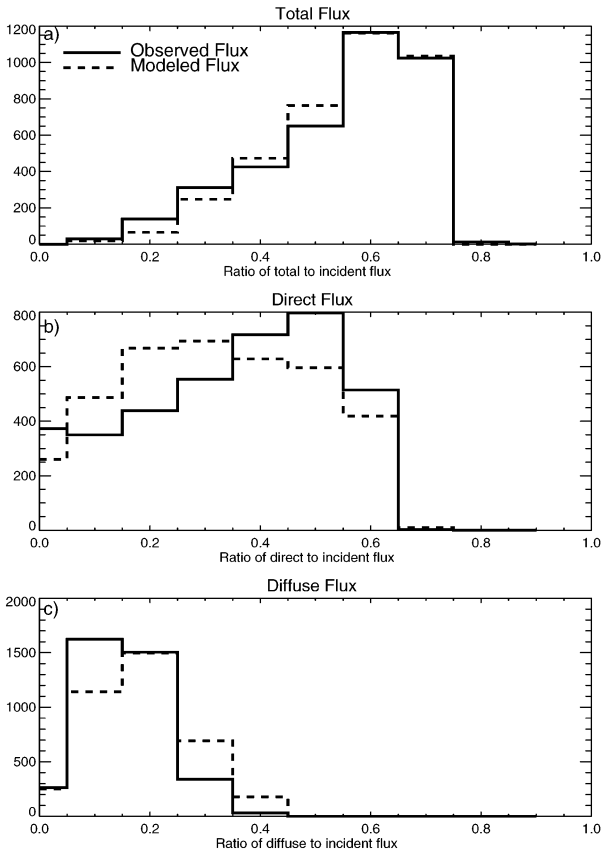

FIG. 7. Ratios of (a) total, (b) direct, and (c) diffuse flux to model flux incident at the top of the atmosphere.

retrieved cloud frequency used in the model is higher than is implicit in the radiation measurements. This trend of the retrievals overestimating cloud amount can also be seen in histograms of the ratio of the observed and modeled fluxes to the model incident flux at the top of the atmosphere. Clear-sky periods are indicated radiatively by high ratios for the direct flux and low ratios in the diffuse flux, while cloudy sky periods have the opposite behavior. In Fig. 7, the modeled fluxes show fewer periods indicative of clear sky (fewer bins with high values of the direct ratio) and more periods indicative of cloudy sky (more bins with high values of the diffuse ratio) than the observations. In the next section, we explore several possible reasons why the retrieved radar cloud amount used in the model is greater than the radiative cloud amount.

6. Cloud amount issues

a. Radar/TSI cloud amount comparison

We evaluate the radar derived cloud amounts used in the model calculations by comparing them to the cloud amount detected by the Total Sky Imager (TSI) from 1–15 July 1999. The TSI is a full-color sky imager that uses a digital camera, which is mounted looking downward to a rotating hemispheric mirror (Long et al. 2001). Images are taken once per minute. We compare the percentage of times that cloud was identified in the ARSCL product during the period to the average TSI cloud fraction in the 120° and 160° fields of view for times when the solar zenith angle is less than 70°. As a hemispheric imager, the TSI observes the whole sky and therefore should detect any clouds that could affect the observed surface radiation, unlike the radar, which is a narrow field-of-view sensor.

TABLE 3. ARSCL and TSI cloud amounts.

	ARSCL	Without MPL high clouds	TSI 120° FOV	TSI 160° FOV
Cloud amount	69.4	55.5	41.0	43.8

Table 3 shows the total cloud amounts derived from the concurrent ARSCL and TSI datasets. If thin cirrus clouds, which are detected by the MPL but not the MMCR, are included, the narrow field-of-view sensors detect cloud 69.4% of the time, while the average TSI cloud amounts from the 120° and 160° fields of view are 41.0% and 44.0%, respectively. If we assume that the cirrus clouds that are not detected by the MMCR are quite thin and also might not be detected by the TSI, the ARSCL cloud frequency falls to 55.5%, which is still 10% greater than the TSI cloud fractions. Over a 2-week period, the cloud amount estimate from the narrow field-of-view radar is considerably higher than that from the hemispheric imager. There are several possible reasons for the overestimate of cloud amount by the radar. In this study cloud amount estimates were only averaged over a 2-week period, which is not long enough to completely sample the cloud fields and provide stationary statistics. Additionally, the cloud field could be anisotropic, which would skew the cloud amount statistics. The TSI and MMCR have different sampling techniques, and different definitions of cloud, which lead to discrepancies in the amount of cloud detected by each sensor. However, the TSI sky cover for wide fields of view ought to be larger than the cloud fraction from a vertical sensor due to the effect of cloud sides.

b. Anisotropy of the Nauru cloud field

The MMCR may overestimate the cloud amount relative to the pyranometer/NIP cloud amount due to anisotropy in the boundary layer cloud field caused by the Nauru island effect. Although the cloud plume is probably not important to the large-scale radiation budget in the Tropics, it may have significant local effects that would bias observations taken at Nauru relative to the surrounding ocean. If the clouds form directly over the ARCS site, they could bias the cloud amount estimate from the vertically pointing, narrow field-of-view radar relative to the pyranometer, which has a hemispheric

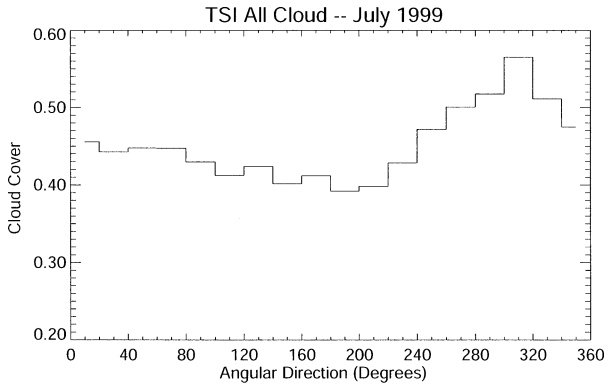

FIG. 8. TSI cloud fraction as a function of compass angle.

field of view, or the NIP, which varies its observation direction over the day.

To examine the possible anisotropy due to the presence of the cloud plume, we examined cloud fraction as a function of azimuthal angle from the 160° FOV TSI imagery during the period 1–15 July 1999. Only images with solar zenith angles less than 60°, which corresponds roughly to the time period 0900 to 1645 LST, are used. For each TSI cloud mask image, we bin the cloud fractions by compass angle in 20° wide bins. Figure 8 shows a histogram of the average cloud fraction as a function of compass angle. There is clearly a peak in cloud fraction around 290°. Although this does not correspond exactly to the average heading of 265° seen by Nordeen et al. (2001) in the GMS data, they do report that ''individual headings ranged from 220° to 320° with a standard deviation of 20°.'' There is not a corresponding peak around 90°–100°, indicating that the boundary layer clouds may form directly over or just downwind of the ARCS site, which would cause a bias in radar cloud fraction relative to the pyranometer/NIP. This analysis shows that the Nauru cloud field is definitely anisotropic, so that one would not necessarily expect the percentage of clouds seen by the zenith-pointing radar to be the same as the percentage of clouds in the direct beam. Over the course of a day at Nauru, the NIP samples azimuthal angles from 80° to 270°.

c. Cloud sampling issues

A second reason that cloud amounts may be too high in the model is the way in which the various remote sensors sample the cloud field. The TSI captures instantaneous sky cover images once per minute. The NIP and PSP measure downwelling fluxes at 1-s intervals, and these measurements are then averaged over 60 s. The MMCR measuring strategy, which is described in more detail in the appendix, is more complicated. The MMCR was designed to detect all radiatively important clouds, ranging from thin boundary layer clouds and cirrus to precipitating clouds. To meet these objectives, a set of four operational modes was designed to allow trade-offs between sensitivity, accuracy, and resolution. Currently, the MMCR cycles through all of the modes in approximately 40 s, spending roughly 9 s on each mode. In the ARSCL product, described by Clothiaux et al. (2000), the reflectivities and Doppler velocities from each of the modes are interpolated onto a 10-s, 45-m time–height grid. Then the best mode at each time and height is chosen, as discussed in the appendix. By interpolating measurements taken ~40 s apart to a 10-s grid and then choosing the best value at each interval, the actual cloud reflectivity may be smeared out in time.

TABLE 4. Boundary layer cloud statistics from ARSCL and mode data.

Dataset	Cloud frequency	Mean LWP* (g m^{-2})
ARSCL	0.47	57.4
Mode 1	0.40	66.3
Mode 3	0.37	87.3

* Liquid water path.

For overcast conditions, this ''smearing'' of the radar reflectivity will affect cloud properties derived from the radar reflectivity data, with the magnitude of the effect depending on the scales at which the cloud properties were variable and the advecting wind speed, but will have little effect on derived cloud amounts. However, for the scattered cumulus prevalent at Nauru, the interpolation has a larger effect on retrieved cloud amount and cloud properties. The average wind speed measured by the National Oceanic and Atmospheric Administration (NOAA) 915-MHz wind profiler at a height of 874 m (which is close to the average retrieved liquid cloud base) over the 3-month period from June through August 1999 was 8.4 m s^{-1}. If the clouds are advecting over the radar at this rate, a smearing of 20 s increases the cloud width by an average of 168 m on either side, which can substantially increase the cloud fraction of these small cumulus. Since the presence of cloud in the model decreases the modeled direct flux and increases the modeled diffuse flux relative to clear sky, an increased cloud frequency in the model relative to the true cloud frequency will tend to cause an underestimate of direct flux and an overestimate of diffuse flux, consistent with the model results presented in section 5.

To examine the possibility that the interpolation of the data for the creation of the ARSCL product causes an overestimate of cloud amount, we compare the observed frequency of boundary layer cloud (heights < 3 km) from the ARSCL data and the individual mode data. Table 4 shows the percentage of time that valid radar reflectivities at heights ≤ 3 km existed within the column for the ARSCL dataset, which were identified as coming from mode 1 (boundary layer mode) or mode 3 (general mode) and for the mode-1 and -3 datasets. Only modes 1 and 3 are examined because they are the modes that are significant for boundary layer clouds.

As expected, mode 1, which is more sensitive, detects boundary layer cloud more often than mode 3. However,

in both cases where the single mode data are used, a lower cloud frequency is observed compared to the ARSCL data. Also shown in Table 4 is an average liquid water path for the three datasets. Since the Bayesian retrieval requires the MWR brightness temperatures, which are on a 20-s grid, while the mode data are not on a regular time grid, we estimate the liquid water content (LWC) as a function of reflectivity for each range gate using a lookup table derived from the Bayesian results. The liquid water path for each column is then calculated. Both of the single mode datasets have higher average liquid water path than the ARSCL dataset. The average mode-3 liquid water path is higher than the mode 1 value, because mode 3 does not detect some regions of thinner cloud or smaller droplets detected by the more sensitive mode 1. The higher retrieved liquid water path from the noninterpolated mode datasets, along with the decreased cloud frequency, supports the idea that the interpolation to the ARSCL grid smears out the clouds, thinning them. Due to the nonlinear nature of radiative transfer, the fluxes calculated from averaged cloud properties are not the same as the average flux calculated from nonaveraged cloud properties. In particular, the presence or absence of a cloud in the model has the largest effect on the modeled direct and diffuse fluxes so that getting the cloud frequency right is very important in modeling the direct and diffuse components of the surface flux.

Although the single mode data do not have the interpolation issues of the ARSCL dataset, the observed reflectivity is still based on a 9-s sample, which does not completely resolve the variability in the boundary layer clouds at Nauru. The PSP and NIP instruments measure downwelling fluxes at 1-s intervals. These measurements are then averaged to 60 s, and only the mean, minimum, maximum, and standard deviation of the 1-s measurements are reported. The top panel in Fig. 9 shows the 60-s mean direct flux from the NIP over an 8-h period on 14 July 1999, while the bottom panel shows the standard deviation of the fluxes measured during each 60-s period. During cloudy periods, the standard deviation of the direct flux measurements within the 60-s period can be as large or larger than the average fluxes, due to the variability of the clouds. For the diffuse flux, the standard deviations over the 60-s interval are usually much smaller than the average fluxes since the observed diffuse flux is a function of the entire cloud field. Over 8 months of observations, the average standard deviation of the NIP measurements within the 60-s interval is 13.3% of the average measured flux and the average standard deviation of the shaded PSP measurements is 3.2% of the average measured flux.

The large standard deviations in the NIP 1-min fluxes indicate that sampling time scales much less than a minute are needed to resolve the variability of the boundary layer clouds at Nauru. If the mode data are used at their original sampling times, and not interpolated onto the ARSCL grid, each mode is sampled every 40 s

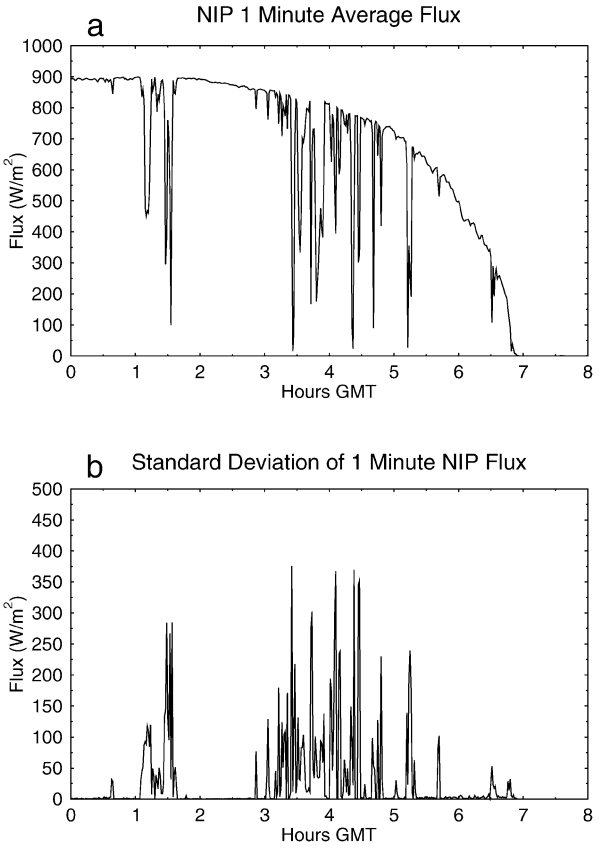

FIG. 9. Average and standard deviation of observed direct flux over 60-s interval.

(although the sampling itself takes ~9 s for each mode), which corresponds to 336-m resolution. Fair weather cumulus generally show variability at higher resolution. Aircraft penetrations of shallow cumulus during the Small Cumulus Microphysics Study (SCMS) experiment show significant changes in LWC and number concentration measured with in situ probes at scales less than 100 m (French et al. 2000). Kollias et al. (2001) studied updrafts and turbulence in fair weather cumuli over Florida using a 94-GHz radar with a sampling interval of 4.5 s. They found that the cumuli studied had updraft cores of ~250–300-m horizontal extent surrounded by downdrafts of ~150-m horizontal extent. Malinowski and Zawadzki (1993) measured the fractal properties of the cloud–clear interface with high-resolution microphysical in situ data in nonprecipitating fair weather cumulus during the Eulerian model Evaluation Field Study at North Bay, Ontario. Based on droplet number concentration and liquid water content measured during two flights in which ~17 and ~10 shallow cumulus clouds were penetrated, they estimated the length of clear and cloudy segments within the flights. Significant numbers of clear-sky regions as narrow as 10 m were seen between cloud segments during the flights. These studies show that shallow cumulus are

TABLE 5. Average uncertainty on retrieved parameters from Bayesian algorithm.

Variable	Average value	Average uncertainty	Average percent uncertainty
LWP	42.7 g m^{-2}	14.4 g m^{-2}	34%
τ	7.2	2.9	40%
LWC	0.092 g m^{-3}	0.05 g m^{-3}	54%
r_e	7.5 μm	0.4 μm	5%

variable on time and spatial scales that cannot be sampled with the current configuration of the MMCR.

The sampling rate and mode configuration of the MMCR was motivated by the speed of the current signal processor, which is not efficient enough to process all of the data taken. At SGP, the efficiency of the radar signal processor is only 4% for mode 4, and increases up to 31% for mode 1 (Clothiaux et al. 1999). A new, faster signal processor is being developed for the MMCRs. These results show that some of this processing power should be put to use by increasing the sampling time for the boundary layer modes. The dwell time of mode 1 should be reduced, the sampling interval should be decreased at least to 10 s (which would allow roughly 84-m horizontal resolution, given the average wind speed) and preferably even further, and the measured parameters of the boundary layer clouds should not be interpolated, which tends to smear them out and artificially increase cloud amount.

d. Uncertainty in cloud property retrievals

A final possibility for the overestimation of retrieved cloud amount is that radar/radiometer-derived cloud properties may not be equivalent to the radiatively important cloud properties. Radar reflectivity is proportional to the sixth moment of the droplet size distribution. In cloud property retrievals, the sixth moment must be related to the radiatively important second and third moments. In the Bayesian retrieval described in Part I, the prior probability distribution function (PDF) derived from aircraft in situ data and the MWR brightness temperatures are used to relate the moments. However, for thin clouds with low liquid water paths, little information is available from the MWR, and most of the constraining information comes from the prior PDF.

In Table 5, the average retrieved values and the average uncertainty in the retrieved values are given for the 12 months of cloud retrievals at Nauru. The average uncertainty in τ, the most radiatively important variable, is 40% of the retrieved value. At low values of τ, changes in τ can produce much larger changes in direct and diffuse flux than in total flux. Thus, it is possible to get the total flux more or less correct while having biases of opposite signs in direct and diffuse flux if estimates of τ are biased for low values of τ. To improve retrievals for low τ, uncertainty in the MWR measurements must be reduced, perhaps by adding a channel near 90 GHz, which has been shown to improve the accuracy of LWP retrievals (Crewell and Löhnert 2003), or by using another type of sensor to determine optical depth for thin clouds. Given the extensive use of dual-channel radiometers, the uncertainty in retrieved liquid water path at low optical depths needs to be accounted for in retrieval algorithms.

7. Conclusions

Ten months of surface observations and retrieved cloud properties at Nauru were combined with a state-of-the-art radiative transfer model to estimate the effect of clouds on the shortwave fluxes at the surface and to perform a flux closure study. The modeled total and direct fluxes agreed with the observations within the stated uncertainty for clear-sky conditions, although the model overestimated the diffuse flux by an average of 17 W m^{-2}. For the study period, an average shortwave cloud radiative effect of -55.4 W m^{-2} was found. The estimates of the shortwave cloud radiative effect at the surface were significantly lower than cloud radiative effect estimates from the TOGA COARE period. The difference is primarily due to the phase of ENSO during the two observational periods. During TOGA COARE, the tropical western Pacific was experiencing a weak El Niño, which generally results in more convection over Nauru, while the current study was a period of suppressed convection during a weak to moderate La Niña. The difference in the cloud radiative effect estimates over the two periods shows the profound influence that ENSO has on the shortwave radiation budget in the Tropics and underscores the need for consistent long-term time series of observations of clouds and radiation in this region.

The flux closure study was performed to test whether cloud properties retrieved from narrow field-of-view, vertically pointing remote sensors are consistent with the measured surface radiation. On short time scales, the modeled and observed surface fluxes showed large differences, due primarily to the large temporal and spatial variability of the cloud field. Averaging over periods as short as 1 h reduced the rms difference in the total fluxes to ~10% of the total observed flux. These results show that statistically the retrieved cloud properties can be used to reproduce the observed downwelling total shortwave flux at the surface within 10%. Thus, statistical comparisons of the retrieved cloud properties with values predicted by cloud-resolving models or general circulation models can be useful in assessing modeled cloud properties.

In general, the modeled total downwelling fluxes were unbiased with respect to the observed fluxes. However, the model tended to underestimate the direct flux and overestimate the diffuse flux. These tendencies can be explained by geometrical arguments for periods with low cloud amount, but as cloud amount increases the continued trend implies that the retrieved cloud amount

used in the model is larger than the radiatively important cloud amount.

The radar cloud amount was compared to the Total Sky Imager (TSI) cloud fraction over a 2-week period and the radar cloud amount was found to be significantly larger. Examination of the TSI cloud decision images indicated that the cloud field was clearly anisotropic, with a peak in cloud amount near a heading of 290°. The anisotropy is assumed to be due to the island-induced cloud plume, which had a general heading toward the west during the study period due to the prevalent easterly trade winds. The radar data were also examined to assess the effect on the retrieved cloud amount and optical depth of interpolating the data from each of the operating modes into one product. It was shown that using the single mode data led to lower cloud amounts and higher liquid water paths than using the ARSCL product, indicating that the interpolation in the ARSCL product tends to artificially increase cloud amount for broken cloud scenes. Examination of the variability in the direct fluxes observed by the NIP indicated that increased sampling frequency is needed to fully resolve the shallow cumulus that are prevalent at Nauru. Additionally, the uncertainty in the MWR brightness temperatures for the shallow cumulus clouds led to large uncertainties in retrieved optical depths. Since the liquid water path or optical depth is a strong constraint on relating the radar reflectivity to the more radiatively important moments of the droplet size distribution, the addition of a third channel to the MWR or another method for retrieving liquid water path of thin clouds is needed to improve the accuracy of remote sensing retrievals.

Acknowledgments. The authors thank Dr. Charles Long and Dr. Roger Marchand for their helpful suggestions on a rough draft of this manuscript. We also thank Dr. Charles Zender and an anonymous reviewer whose thoughtful comments have improved the manuscript. The majority of this research was undertaken while the first author was a graduate student at the University of Colorado. The research was supported by the Office of Biological and Environment Research of the U.S. Department of Energy (under Grant DE-A1005-90ER61069 to the NASA Goddard Space Flight Center and Contract DE-AC06-76RL01830 to Pacific Northwest National Laboratory) as part of the Atmospheric Radiation Measurement program. The Pacific Northwest National Laboratory is operated by Battelle for the U.S. Department of Energy. The first author was also supported in part by a National Science Foundation Graduate Research Fellowship.

APPENDIX

Details of MMCR Processing

Clothiaux et al. (1999) details the current operational modes at the ARM sites and the design justifications for each mode. Mode 1, the boundary layer mode, is tuned to detect weakly reflecting low-level clouds. Mode 2, the cirrus mode, is tuned to detect higher-level weakly reflecting clouds, and has a minimum range of 2985 m, due to pulse coding. Mode 3, the general mode, was designed to be fairly sensitive to all clouds at all altitudes, while mode 4, the robust mode, produces accurate reflectivities and velocities from particles with large fall speeds.

In the current configuration, the MMCR cycles through all of the modes in approximately 40 s, spending roughly 9 s on each mode. Due to the speed of the current signal processor and the necessity of pulse coding, coherent averaging, and other processing, the computer cannot process all of the data generated by the radar. For example, the current boundary layer mode at Nauru has a dwell time of only 2.3 s, but that dwell time is evenly distributed across the 9-s processing period (E. Clothiaux 2002, personal communication).

In the ARSCL product, described by Clothiaux et al. (2000), the reflectivities and Doppler velocities from each of the modes are merged onto a 10-s, 45-m time–height grid. This merging is accomplished by linearly interpolating the measured radar reflectivity, Doppler velocity, and Doppler spectral width from each mode onto the grid. Then the best mode at each time and height is chosen based on minimizing coherent averaging, second trip echo, and pulse coding problems, using measurements with high signal-to-noise ratios, and attempting to produce contiguous regions from a single mode. Data from the general mode (mode 3) is used preferentially, except in regions of weak radar reflectivities where the signal-to-noise ratio in mode 3 is less than 5 dB (in which case mode-1 or -2 data is used) and regions of fast moving hydrometeors (in which case mode-4 data is used). Mode 2 values are never used for boundary layer clouds since the lowest range gate for this mode is at 2.985 km, and mode-4 data will generally only be used for boundary layer clouds near regions of precipitation. Thus, for boundary layer clouds, the best gridded value, which is the reflectivity value in the ARSCL product, is often interpolated from a mode 1 or mode 3 value.

REFERENCES

Ackerman, T. P., D. M. Flynn, and R. T. Marchand, 2003: Quantifying the magnitude of anomalous solar absorption. *J. Geophys. Res.,* **108,** 4273, doi:10.1029/2002JD002674.

Chou, M.-D., and W. Zhao, 1997: Estimation and model validation of surface solar radiation and cloud radiative forcing using TOGA COARE measurements. *J. Climate,* **10,** 610–620.

Clothiaux, E. E., and Coauthors, 1999: The Atmospheric Radiation Measurement Program cloud radars: Operational modes. *J. Atmos. Oceanic Technol.,* **16,** 819–827.

——, T. P. Ackerman, G. G. Mace, K. P. Moran, R. T. Marchand, M. A. Miller, and B. E. Martner, 2000: Objective determination of cloud heights and radar reflectivities using a combination of active remote sensors at the ARM CART sites. *J. Appl. Meteor.,* **39,** 645–665.

Clough, S. A., and M. J. Iacono, 1995: Line-by-line calculation of

atmospheric fluxes and cooling rates. 2: Application to carbon dioxide, ozone, methane, nitrous oxide, and the halocarbons. *J. Geophys. Res.,* **100,** 16 519–16 535.
——, ——, and J.-L. Moncet, 1992: Line-by-line calculation of atmospheric fluxes and cooling rates: Application to water vapor. *J. Geophys. Res.,* **97,** 15 761–15 785.
Crewell, S., and U. Löhnert, 2003: Accuracy of cloud liquid water path from ground-based microwave radiometery. Part 2: Sensor accuracy and synergy. *Radio Sci.,* **38,** 8042, doi:10.1029/2002RS002634.
d'Almeida, G. A., P. Koepke, and E. P. Shettle, 1991: *Atmospheric Aerosols: Global Climatology and Radiative Characteristics.* A. Deepak, 561 pp.
Dong, X., T. P. Ackerman, E. E. Clothiaux, P. Pilewskie, and Y. Han, 1997: Microphysical and radiative properties of boundary layer stratiform clouds deduced from ground-based measurements. *J. Geophys. Res.,* **102,** 23 829–23 843.
——, P. Minnis, G. G. Mace, W. L. Smith, M. Poellot, R. T. Marchand, and A. D. Rapp, 2002: Comparison of stratus cloud properties deduced from surface, GOES, and aircraft data during the March 2000 ARM cloud IOP. *J. Atmos. Sci.,* **59,** 3265–3284.
Evans, K. F., 1998: The spherical harmonics discrete ordinate method for three-dimensional atmospheric radiative transfer. *J. Atmos. Sci.,* **55,** 429–446.
Feingold, G., W. L. Eberhard, D. E. Veron, and M. Previdi, 2003: First measurements of the Twomey indirect effect using ground-based remote sensors. *Geophys. Res. Lett.,* **30,** 1287, doi:10.1029/2002GL016633.
French, J. R., G. Vali, and R. D. Kelly, 2000: Observations of microphysics pertaining to the development of drizzle in warm, shallow cumulus clouds. *Quart. J. Roy. Meteor. Soc.,* **126,** 415–443.
Frisch, A. S., C. W. Fairall, and J. B. Snider, 1995: Measurement of stratus cloud and drizzle parameters in ASTEX with a K_a-band Doppler radar and a microwave radiometer. *J. Atmos. Sci.,* **52,** 2788–2799.
Haeffelin, M., S. Kato, A. M. Smith, C. K. Rutledge, T. P. Charlock, and J. R. Mahan, 2001: Determination of the thermal offset of the Eppley precision spectral pyranometer. *Appl. Opt.,* **40,** 472–484.
Halthore, R. N., and S. E. Schwartz, 2000: Comparison of model-estimated and measured diffuse downward irradiance at surface in cloud-free skies. *J. Geophys. Res.,* **105,** 20 165–21 077.
——, ——, J. Michalsky, G. Anderson, R. Ferrare, B. Holben, and H. T. Brink, 1997: Comparison of modeled estimated and measured direct-normal solar irradiance. *J. Geophys. Res.,* **102,** 29 991–30 002.
Kato, S., T. P. Ackerman, E. E. Clothiaux, J. H. Mather, G. G. Mace, and M. L. Wesely, 1997: Uncertainties in modeled and measured clear-sky surface shortwave irradiances. *J. Geophys. Res.,* **102,** 25 881–25 898.
Kollias, P., B. Albrecht, R. Lhermitte, and A. Savtchenko, 2001: Radar observations of updrafts, downdrafts, and turbulence in fair-weather cumuli. *J. Atmos. Sci.,* **58,** 1750–1766.
Li, Z., A. Trischenko, H. Barker, G. Stephens, and P. Partain, 1999: Analyses of Atmospheric Radiation Measurement (ARM) program's Enhanced Shortwave Experiment (ARESE) multiple data sets for studying cloud absorption. *J. Geophys. Res.,* **104,** 19 127–19 134.
Long, C. N., 1996: Surface radiative energy budget and cloud forcing: Results from TOGA COARE and techniques for identifying and calculating clear sky irradiance. Ph.D. thesis, The Pennsylvania State University, 193 pp.
——, and T. P. Ackerman, 2000: Identification of clear skies from broadband pyranometer measurements and calculation of downwelling shortwave cloud effects. *J. Geophys. Res.,* **105,** 15 609–15 626.
——, D. W. Slater, and T. Tooman, 2001: Total sky imager model 880 status and testing results. Tech. Rep. ARM TR-006, 36 pp.
Mace, G. G., and K. Sassen, 2000: A constrained algorithm for retrieval of stratocumulus cloud properties using solar radiation, microwave radiometer, and millimeter cloud radar data. *J. Geophys. Res.,* **105,** 29 099–29 108.
Malinowski, S. P., and I. Zawadzki, 1993: On the surface of clouds. *J. Atmos. Sci.,* **50,** 5–13.
Mather, J., T. Ackerman, W. Clements, F. Barnes, M. Ivey, L. Hatfield, and R. Reynolds, 1998: An atmospheric radiation and cloud station in the tropical western Pacific. *Bull. Amer. Meteor. Soc.,* **79,** 627–642.
McClatchey, R. A., R. W. Fenn, J. A. Selby, F. E. Volz, and J. S. Garing, 1972: Optical properties of the atmosphere. 3d ed. Environmental Research Paper 411, Air Force Cambridge Research Laboratories, 411 pp.
McFarlane, S. A., and K. F. Evans, 2004: Clouds and shortwave fluxes at Nauru. Part I: Retrieved cloud properties. *J. Atmos. Sci.,* **61,** 733–744.
——, ——, and A. S. Ackerman, 2002: A Bayesian algorithm for the retrieval of liquid water cloud properties from microwave radiometer and millimeter radar data. *J. Geophys. Res.,* **107,** 4317, doi:10.1029/2001JD001011.
McFarquhar, G. M., and A. J. Heymsfield, 1996: Microphysical characteristics of three anvils sampled during the Central Equatorial Pacific Experiment. *J. Atmos. Sci.,* **53,** 2401–2423.
——, ——, J. Spinhirne, and B. Hart, 2000: Thin and subvisual tropopause tropical cirrus: Observations and radiative impacts. *J. Atmos. Sci.,* **57,** 1841–1853.
Michalsky, J., E. Dutton, D. Nelson, M. Rubes, T. Stoffel, M. Wesley, M. Splitt, and J. DeLuisi, 1999: Optimal measurement of surface shortwave irradiance using current instrumentation. *J. Atmos. Oceanic Technol.,* **16,** 55–69.
Mlawer, E. J., S. J. Taubman, P. D. Brown, M. J. Iacono, and S. A. Clough, 1997: Radiative transfer for inhomogeneous atmospheres: RRTM, a validated correlated-k model for the longwave. *J. Geophys. Res.,* **102,** 16 663–16 682.
——, S. A. Clough, and S. Kato, 1998: Shortwave clear sky model measurement intercomparison using RRTM. *Proc. Seventh Atmospheric Radiation Measurement (ARM) Science Team Meeting,* San Antonio, TX, U.S. Department of Energy, 513–516.
——, P. D. Brown, S. A. Clough, L. C. Harrison, J. J. Michalsky, P. W. Kiedron, and T. Shippert, 2000: Comparison of spectral direct and diffuse solar irradiance measurements and calculations for cloud-free conditions. *Geophys. Res. Lett.,* **27,** 2653–2656.
Moran, K. P., B. E. Martner, M. J. Post, R. A. Kropfli, D. C. Welsh, and K. B. Widener, 1998: An unattended cloud-profiling radar for use in climate research. *Bull. Amer. Meteor. Soc.,* **79,** 443–455.
Nordeen, M. L., P. Minnis, D. R. Doelling, D. Pethick, and L. Nguyen, 2001: Satellite observations of cloud plumes generated by Nauru. *Geophys. Res. Lett.,* **28,** 631–634.
Pincus, R., and S. A. Klein, 2000: Unresolved spatial variability and microphysical process rates in large-scale models. *J. Geophys. Res.,* **105,** 27 059–27 065.
Shiobara, M., and S. Asano, 1994: Estimation of cirrus optical thickness from sun photometer measurements. *J. Appl. Meteor.,* **33,** 672–681.
Smirnov, A., B. N. Holben, Y. J. Kaufman, O. Dubovik, T. F. Eck, I. Slutsker, C. Pietras, and R. N. Halthore, 2002: Optical properties of atmospheric aerosol in maritime environments. *J. Atmos. Sci.,* **59,** 501–523.
Takano, Y., and K.-N. Liou, 1989: Solar radiative transfer in cirrus clouds. Part I: Single-scattering and optical particles of hexagonal ice crystals. *J. Atmos. Sci.,* **46,** 3–19.
Warner, J. X., and R. G. Ellingson, 2000: A new narrowband radiation model for water vapor absorption. *J. Atmos. Sci.,* **57,** 1481–1496.
Yang, P., K. N. Liou, K. Wyser, and D. Mitchell, 2000: Parameterization of the scattering and absorption properties of individual ice crystals. *J. Geophys. Res.,* **105,** 4699–4718.
Zender, C. S., B. Bush, S. K. Pope, A. Bucholtz, W. D. Collins, J. T. Kiehl, F. P. J. Valero, and J. Vitko Jr., 1997: Atmospheric absorption during the Atmospheric Radiation Measurement (ARM) Enhanced Shortwave Experiment (ARESE). *J. Geophys. Res.,* **102,** 29 901–29 915.